energies

MDPI

Article

Acoustic Triggering of Combustion Instability in a Swirling Flame: An Experimental Study

Yunpeng Liu [1,2], Yingwen Yan [1,*], Shoutang Shang [2] and Hongyu Ma [2]

[1] College of Energy and Power Engineering, Nanjing University of Aeronautics and Astronautics, Nanjing 210016, China; ypliu@nuaa.edu.cn
[2] Shenyang Aero Engine Research Institute, Aero Engine Corporation of China, Shenyang 110066, China; gssst606@163.com (S.S.); mahongyu1973@163.com (H.M.)
* Correspondence: yanyw@nuaa.edu.cn; Tel.: +86-137-7050-7240

Abstract: Combustion instability is a common thermoacoustic coupling problem in combustion systems, and the pressure oscillations generated inevitably damage the combustion system. Studying the mechanism of combustion instability, especially the triggering problem of combustion instability, is particularly important for understanding combustion instability. This article adopts experimental research methods. The flame transfer function and flame describing function governing pressure pulsation were hereby measured to study the effect of heat release rate fluctuation on acoustic disturbance. By triggering combustion instability through ignition, the growth process of combustion instability was also studied. The results showed that flame pulsation amplitude shows a complex curvature when the frequency is lower than 200 Hz, while the growth rate of pulsation amplitude monotonically decreases as frequencies increase above 200 Hz. According to the considerable self−excited combustion instability tests, the oscillation amplitudes in the limit cycle state are generally greater than 0.4, while the pressure amplitudes in the limited state are less than 0.2, thus verifying the concept of a trigger threshold for low−frequency oscillation. In addition, analysis of the growth rate, the pressure and the attractor of the heat release pulsation observed after the triggering of combustion instability reveals that the triggering of combustion instability is a gradual coupling process between oscillation pressure and heat release rate pulsation.

Keywords: combustion instability; flame driving characteristics; rayleigh integration; heat release rate pulsation; combustion instability mechanism

Citation: Liu, Y.; Yan, Y.; Shang, S.; Ma, H. Acoustic Triggering of Combustion Instability in a Swirling Flame: An Experimental Study. *Energies* **2023**, *16*, 5568. https://doi.org/10.3390/en16145568

Academic Editors: Peiyong Wang and Fei Xing

Received: 29 June 2023
Revised: 17 July 2023
Accepted: 20 July 2023
Published: 23 July 2023

1. Introduction

Swirling combustion technology, one of the widely applied combustion technologies, contributes considerably to flame stabilization, fuel atomization and effective fuel–air mixture. However, in the event of inlet disturbance and disturbance of the swirling flow field, the combustion rate can become coupled with sound pressure pulsations to form a self−perpetuating combustion instability. The development of high−fuel/air−ratio (FAR) and fuel−lean combustors has made combustion instability an increasingly serious issue [1]. The flow field disturbance modifies the flame to generate a heat release rate pulsation, which drives the gas to produce a pressure wave. After reflection from the boundary of the combustion chamber, the pressure wave couples with the heat release rate pulsation, thereby establishing a strong combustion oscillation. The amplitude of these oscillations may increase until some limit state is reached.

For engineering practice, the latest work provides a numerical tool of analyzing thermoacoustic systems [2]. It could be applied to predict the acoustic signature of the combustor and to examine and evaluate the performance self−sustained thermoacoustic oscillations. Zhao systematically proposed the mechanism and control of combustion instability [3]. In addition, the suppression of oscillating combustion is particularly important.

However, currently, it is difficult to find practical applications for most inhibition studies, such as inputting anti−phase sound waves [4] or CO_2 jets [5,6] into combustion systems to suppress oscillating pressure. Passive suppression methods for industrial applications are gradually being established [7,8]. Furthermore, in any case, the mechanisms of combustion instability are extremely important for suppression research. The coupling of the combustion instability with the flow field, combustion field and sound field presents extremely complex patterns of physical and chemical behavior. When the heat release rate pulsation couples with the flow field and vortex structure [9], the stability of the flamelet will be affected. As the heat release rate pulsation also has a pressure component, the acoustic impedance characteristics of the system exercise a significant impact on the characteristics of the resulting combustion instability [10]. Ducruix et al. [11] summarized relevant studies on the early acoustics/flame/vortex and other coupling mechanisms. In recent studies, numerical simulations have often been used to investigate the mechanisms of combustion field pulsation [12,13]. Numerical simulations make it easier to assess the physical parameters in the combustion flow field, such as the fluctuations in flame heat output, at high spatial–temporal resolution. In addition, numerical simulations generate relatively realistic dynamic models of the coupling of sound waves and flame in annular combustion chambers [14].

To facilitate numerical solutions, it is generally necessary to simplify the acoustic boundary and the overall dynamic model [15,16]. Therefore, numerical simulations may fail to truly simulate the thermoacoustic coupling process. Certain inlet conditions may suffice to generate a spontaneous self−exciting combustion instability [17,18], and it exhibits large oscillation amplitude in the nonlinear region [19]. Parameters such as equivalence ratio and thermal power have significant impacts on chemical and thermodynamic characteristics, thereby affecting combustion instability [20]. Combustion instability can be predicted by means of pressure signal analysis [21]. However, the self−exciting combustion instability may also reach the limit cycle state quickly; then, an external source of excitation is generally required for empirical test research [22,23]. Externally exciting sound waves may be used to carry out a quantitative investigation of the laws linking the growth of flame pulsation energy to disturbance amplitude. The energy pulses given off by the flame increase with the disturbance amplitude, and the observation of this can be charted to reveal the initial triggering of the combustion instability, its subsequent growth and ultimate oscillation saturation.

To reiterate the essential mechanism, whether the process is externally forced or not, flame pulsation is the ultimate driving force of the pressure oscillations, which may, in turn, feed back to further enhance the amplitude of the heat release rate pulsation. The spectral response of the flame upon acoustic agitation is commonly known as the flame transfer function (FTF), and the amplitude response of the flame upon acoustic agitation is correspondingly known as the flame describing function (FDF). FTF/FDF is constrained by the flame shape [24], thermal power rates and equivalence ratios [25]. Although studies on FTF and FDF have been performed to predict combustion instability [26], the mechanisms through which FTF and FDF may contribute to combustion instability have not yet been articulated.

In practice, FTF is studied to interpret the triggering and development of combustion instability, and to combine with the system's acoustic characteristics to establish a closed−loop system. The transfer function describes the dynamic behaviors of the combustion, which may then be applied to the forecasting of combustion instability [27]. In general, the FTF is combined with the thermoacoustic network model, and the resulting low−order model is applied to analyze the impact of the flame response to the combustion instability [28]. In addition, the FTF and the FDF can be used to predict the dominant frequency and amplitude of the combustion instability. For example, Campa et al. [29] compared and studied the influences of spatially distributed flames and compact ideal flames on calculated thermoacoustic stability using the Reynolds average method. Through analysis of the effect of the FTF of the flame pulsation on the sound wave velocity disturbance, it was revealed that the characteristic frequency was most consistent with the dominant frequency of the combustion instability. Han et al. [30] predicted the coupling strength of the flame to the feedback characteristics of the sound wave disturbance using a numerical simulation method.

On the other hand, FDF is often used to analyze the non−linear characteristics of combustion instability. For example, Kim et al. [22] studied the influence of non−linear dynamics on the combustion instability of a coaxial jet flame; an FDF experiment was conducted to establish the non−linear model. Eirik et al. [31] explored the non−linear response characteristics for different nozzle spacings and hydrogen enrichment levels by measuring the FDF close to the frequency of the self−excitation mode in a combustion chamber. Kim et al. [32] analyzed the triggering of combustion instability by using the relatively complete analysis method in combination with FTF and FDF; however, there remained a degree of imprecision associated with the use of a photomultiplier tube for detecting the overall flame CH* luminous intensity and obtaining the heat release rate pulsation signal.

Gain and phase are generally key indicators for FTF [33], and under small amplitude conditions, it is believed that there is a linear relationship between heat release rate feedback and disturbance [34]. To date, the coupling and triggering mechanisms of combustion instability have taken velocity disturbance and pressure disturbance as input parameters [35,36], an approach that has generated profound insights into the triggering and growth mechanism of combustion instability. However, there have been few studies of the swirling diffusion flame of butane from a porous nozzle. In this paper, we report an investigation of the triggering of combustion instability in a swirling diffusion butane flame and the response characteristics of the flame upon acoustic disturbance, with special regard to the analysis of the flame spectrum and patterns of growth in flame amplitude. The present study included high−frequency photography of the flame and combined this photography with the multidimensional dynamic decomposition method to identify the heat release rate pulsation amplitude. The initial triggering of the combustion instability was also investigated in detail.

2. Materials and Methods

2.1. Experimental System

Figure 1 shows the experimental setup conducted in this research. The combustion instability monitoring system (Figure 1A) includes swirlers for stabilizing the flame, an airflow system, hot−wire anemometer for airflow measurement, fuel supplement system, combustor and signal measurement system. The system is supplied with atmospheric air at room temperature (~17 K). The flame is fed with n−butane at atmospheric pressure. Its density under standard conditions is 2.48 kg/m^3. The stoichiometric FAR of n−butane is 0.064, which is close to that of aviation kerosene (0.068). To facilitate understanding, the actual fuel/air ratios and their associated equivalence ratios used in our tests are presented in Table 1. At the fan outlet, a stilling tank ensured the delivery of smooth airflow by eliminating fan blade pulsations. To study the flame response to pressure disturbance, a loudspeaker was installed at the inlet of the experimental system to create controlled pressure disturbances. Figure 1A shows the specific installed position of the loudspeaker. The driving voltages were varied to adjust the disturbance amplitude. The acoustic signal was continuously stable during the experiment. A high−speed dynamic pressure sensor was installed on the wall of the airflow tube upstream of the swirler.

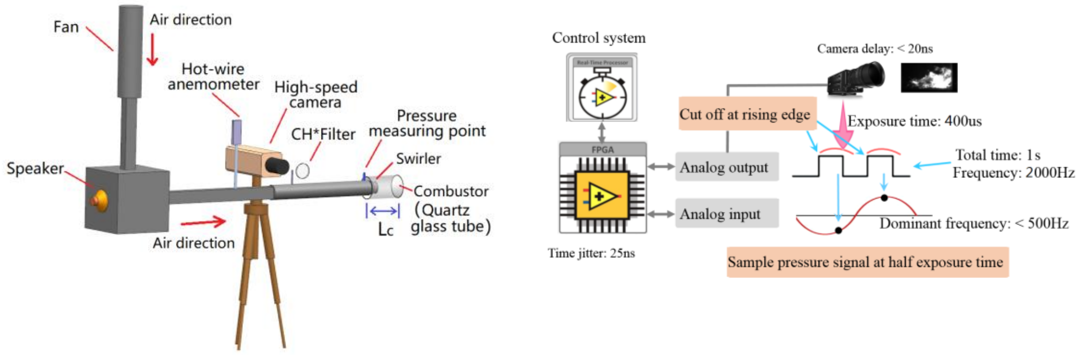

(**A**) Experimental system (**B**) Synchronous sampling control system

Figure 1. Experimental system used in the present study.

Table 1. Test conditions.

Case	Reynolds Number	FAR	ϕ
A	5500	0.0207	0.323
B	5500	0.0241	0.377
C	5500	0.0275	0.430
D	4500	0.0275	0.430

In the research of FTF, it is necessary to prevent the reflection of the speaker−induced sound wave at the outlet of the combustor. Therefore, the length of the combustion chamber (in the form of a quartz glass tube) downstream of the swirler is limited to 100 mm. Such a short pipe causes the acoustic wave to pass through the flame and diffuse to the environment without retro−reflection. For studying the self−excited combustion instability, different combustion chamber lengths were then installed, leading to combustion instabilities with different dominant frequencies and amplitudes. The lengths of the combustor ranged from 500 to 900 mm, and the inner diameter was 100 mm. The flame image was photographed at a high frequency using IDT's Y5 series high−speed camera with a methyl (CH*) filter. The center wavelength was 430 nm, and the bandwidth was 10 nm, the exposure time was 400 µs and the sampling frequency was 2000 Hz. The high−frequency pressure changes upstream of the swirler were measured, in a synchronized manner, while the flame oscillations were being photographed. Figure 1B shows the synchronous control system. The time over which the samples were taken was 1 s, and the pressure was sampled in the middle of each exposure.

Figure 2 shows the swirler and fuel nozzle structure. A porous fuel nozzle was used to establish a diffusion combustion mode. In the central axis direction, the antidromic pressure gradient caused by the swirling centrifugal force helps produce the central recirculation zone, in which the successive flame resides. The counter−swirling air jets promote the mixing of the air and the fuel. Figure 2B shows a three−dimensional half−section of the combustor. A large swirling flow velocity exists in the venturi, and it is a challenge to balance the flame and air velocities. The fuel is gradually mixed with air and burned at the head of the combustor, and the flame in the combustor is mostly blue, with a small amount of orange flame. Due to the high velocity of the swirling jets, the flame mainly exists behind the venturi. The nozzle supplying the fuel to the combustion chamber is of the porous type. The swirl numbers of the primary and secondary swirlers are 1 and 0.8, respectively.

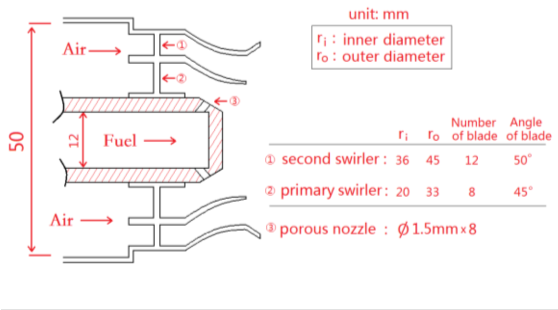

(**A**) Swirler and fuel nozzle structure

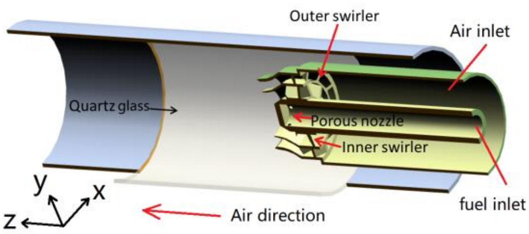

(**B**) Three–dimensional half–section of the combustor

Figure 2. Combustor arrangements.

A hot−wire anemometer was used to measure the air flowrate. Before the experiments, a thermal flowmeter with an accuracy of 0.5% was used to calibrate the anemometer. A calibrated rotameter with an accuracy of 2% was used to the fuel flowrate. An AE−H high−frequency pressure sensor from Nanjing Aire−sensor Technology Co. Ltd. (Nanjing, China) was adopted, with a range of −3 to 3 kPa, an output voltage range of 0~10 v, a comprehensive accuracy of 0.5% and a frequency response range of 0~20 kHz. The inlet test conditions are shown in Table 1, and the test measurement was carried out for four working conditions, of which Case A represents the benchmark control group.

The relationship between the driving voltage of the loudspeaker and the acoustic pressure is measured in a special environment. The verification standard is to ensure that the loudspeaker generates a constant velocity disturbance. Figure 3 shows the loudspeaker calibration system. The loudspeaker is installed at the end of a short tube 30 mm in length. The other end of the tube is closed, meaning that the impedance at the end is infinite. According to acoustic theory, the acoustic impedance at the sensor installation position is $Z_{s0} \approx -j\rho_0 c_0 \cot kl$, where $k = 2\pi f/\omega$ is wave number and l is length. According to $p = v \cdot Z_{s0}$, where v is velocity wave, the acoustic pressure amplitude at the sensor position is $p = \cot 2\pi f l/c_0 \cdot v$. Figure 4 shows the verification results of acoustic pressure amplitude and driving voltage of the loudspeaker when the velocity amplitude is fixed. From this, it appears that the speaker has obvious nonlinear characteristics.

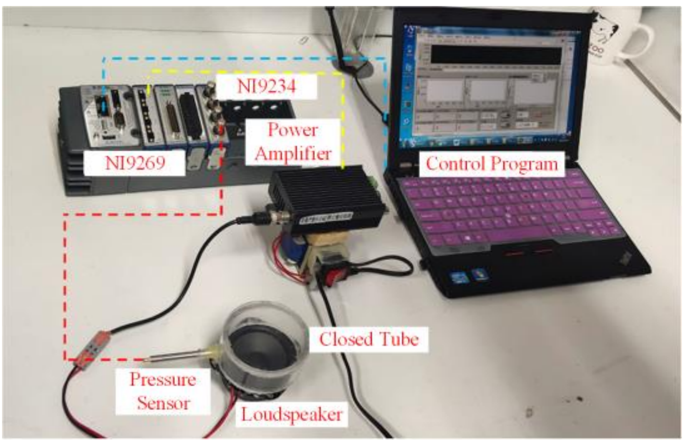

Figure 3. Loudspeaker verification system.

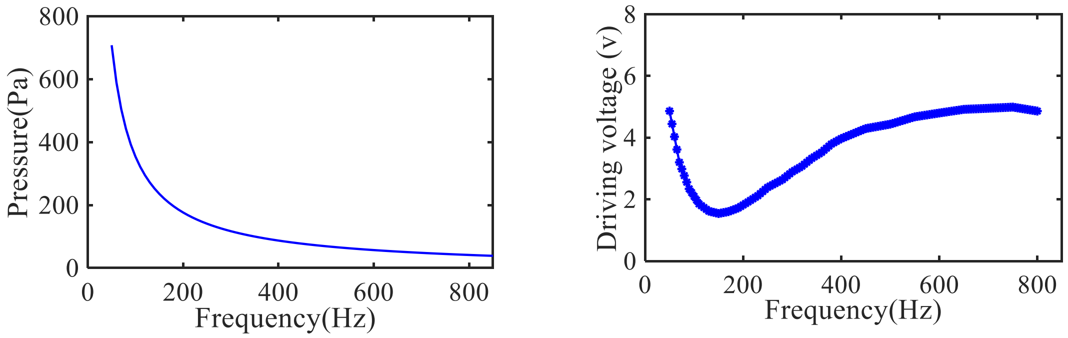

Figure 4. Verification of loudspeaker's driving voltage.

2.2. Data Analysis Methods

Dynamic mode decomposition (DMD) was adopted [37] to complete the mode decomposition of the CH* images and obtain the dominant frequency and the pulsation distribution. Figure 5 shows the DMD results in Case A when subject to a speaker frequency of 250 Hz. The spectral analysis in Figure 5A indicates that the flame pulsation presented a dominant frequency equal to the forcing frequency. Figure 5B shows the amplitude distribution. The unit in the of the original images is the gray value. The results display the pulsation characteristics of the various regions of the flame.

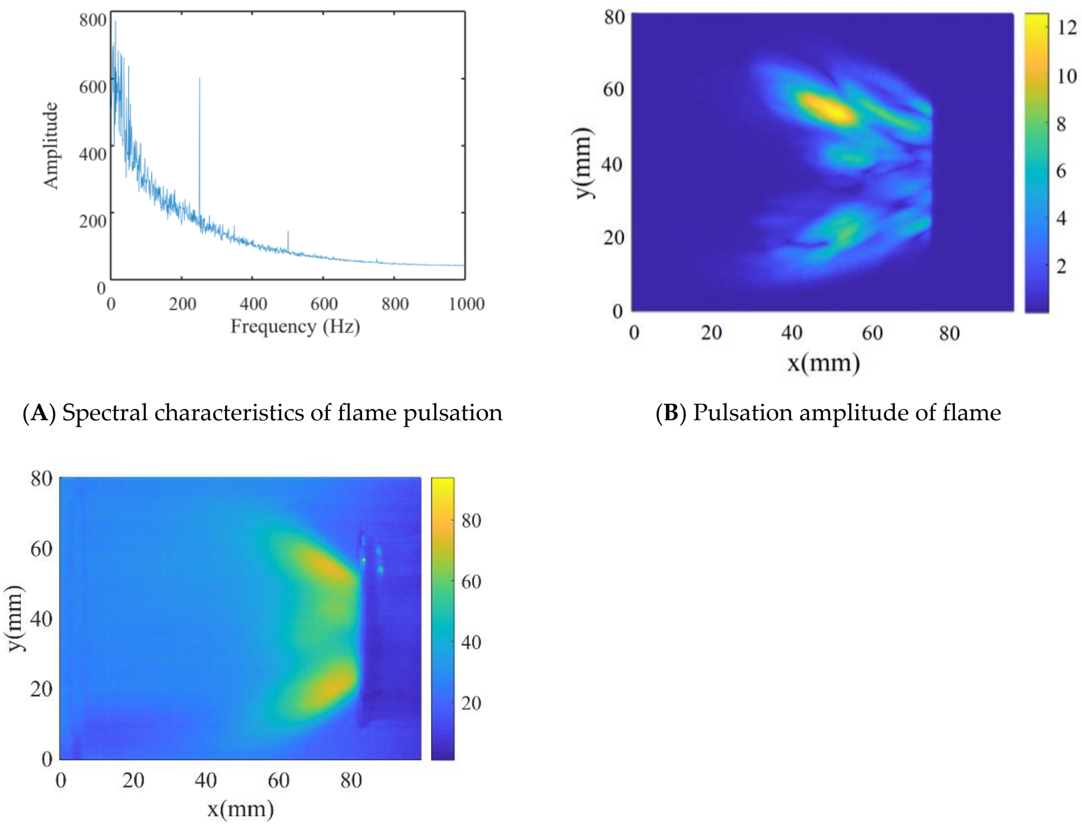

(**A**) Spectral characteristics of flame pulsation

(**B**) Pulsation amplitude of flame

(**C**) Time−averaged flame image

Figure 5. DMD decomposition of flame pulsation in Case A (f = 250 Hz, p_A = 0.1).

In this study, the pulsation values (Q') and time−averaged values ($\overline{Q}$) of heat release rate are derived from CH* images. The continuous pulsating flame images are decomposed through the DMD method to obtain the flame pulsation intensity distribution (Figure 5B) corresponding to the dominant frequency, and then the result is spatially integrated to obtain the amplitude of heat release rate pulsation Q_A. The time−averaged heat release rate (Figure 5C) is obtained by integrating the time−averaged CH* image. Then, the dimensionless heat release rate pulsation intensity can be calculated from $H_A = Q_A/\overline{Q}$. In addition, in this manuscript, only one dynamic pressure sensor is used to measure the pressure pulsation (P_A) and average gauge pressure ($\overline{p}$) at the inlet of the swirler. The dimensionless pressure pulsation amplitude is obtained from the ratio of these two parameters ($p_A = P_A/\overline{p}$) and is used as the input variable of FTF/FDF.

The pulsation parameters exhibited in combustion instability include pressure pulsation, heat release rate pulsation and velocity pulsation. Many studies have taken the velocity pulsation as the input parameter of the flame transfer function. The swirler exhibits a significant blockage effect on the air flow, so in the externally excited and self−excited combustion instability tests, the pressure pulsation upstream of the swirler is employed as the input parameter for flame response. In addition, it is crucial that the pressure signal is easier to measure in the experiment. In the FTF tests, the disturbance amplitude of acoustic pressure was ensured to be constant in the experiment. Although pressure pulsation and velocity pulsation are not synchronized and related to the resonance characteristics of the test system, for FDF, when the disturbance frequency is fixed, the nonlinear fluctuation in heat release rate with the increase in disturbance amplitude should be similar, such as saturation.

The flame pulsation and oscillation pressure signals were standardized, and the dimensionless pressure amplitude p_A is shown in Equation (1):

$$p_A = P_A/\overline{p} \tag{1}$$

where P_A denotes the dynamic pressure amplitude and $\overline{p}$ represents the average gauge pressure. In calculating the strength of the flame heat release rate pulsation, signal processing similar to (1) is required as standard. The pulsation gain of the flame is defined by Equation (2):

$$G = H_A/p_A \tag{2}$$

where H_A is the dimensionless heat release rate pulsation amplitude and p_A refers to the dimensionless amplitude of the acoustic pressure. Cross−correlation technology is adopted to calculate the phase difference between the upstream pressure signal of the swirler and the flame heat release rate pulsation. With regard to two discrete signal sums, i.e., $x(t)$ and $y(t)$, the variance of the two waveforms is solved using Equation (3):

$$\sigma^2 = \frac{1}{n}\sum_{i=1}^{n}(x_i - y_i)^2 \tag{3}$$

The waveform variance is decomposed to

$$\sigma^2 = \frac{1}{n}\sum_{i=1}^{n}(x_i)^2 + \frac{1}{n}\sum_{i=1}^{n}(y_i)^2 - 2\frac{1}{n}\sum_{i=1}^{n}x_i y_i \tag{4}$$

The third item in Equation (4) is the cross−correlation function R_{xy} of the two signals. A greater R_{xy} indicates greater similarity between the two signals. The cross−correlation function of the signal set $x(t)$ at time t is defined as

$$R_{xy}(\tau) = \frac{1}{n}\sum_{i=1}^{n}[x_i(t)y_i(t+\tau)] \tag{5}$$

It is noted that in Equation (5), when $x_i(t) = y_i(t)$, the equation becomes the autocorrelation function, and the period of the signal can then be calculated. The cross−correlation function may also be used for analyzing the communication process of the signals, in which the cross−correlation distance equates to the transmission lag time. The phase difference may be determined by analyzing the lag time between the acoustic pressure and the heat release rate pulsation.

The relative convection time is adopted to describe the phase relations between the pressure pulsation and flame pulsation, i.e., the lag time τ to cycle T ratio, τ/T. In solving for the phase difference between the flame pulsation and the pressure pulsation, the flame surface yields the propagation process of surface waves, indicating the possible presence of multiple flame pulsations in the whole flame pulsation area. Hence, only the local flame in the upstream region of the combustion chamber is used to derive the phase relationship. To guarantee the continuity of the relative convection time, the time at the relevant frequencies exceeds 1, and the phase difference is deemed beyond one period.

In the experiment debugging, the growth process of oscillating pressure and heat release rate is very fast, and it is difficult to catch the growth process in the unstable transition state of combustion by adjusting the working parameters. Therefore, this research adjusts the working parameters to combustion instability state before ignition. Then, combustion instability is triggered through ignition and the growth process is measured. The method of forced ignition can also be found in the literature [37]. In this research, an oscillation pressure amplitude fitting method is proposed to describe the growth rate of oscillating pressure. The mechanism of pressure growth is also described. An exponential fit is applied to the envelope of the pressure signal in the growth period to obtain the growth rate of the oscillation pressure. The exponential fitting formula is shown in Equation (6).

$$A(t) = \alpha e^{\beta t} + \gamma \tag{6}$$

where $A(t)$ denotes the oscillation pressure amplitude changing with time, α the pre−exponential factor, β the exponential factor, γ the average value, the derivative $A'(t)$ is termed the growth rate of the oscillation pressure amplitude and $\alpha \cdot \beta$ is the initial growth rate.

3. Results and Discussion

3.1. FTF (Spectral Response of the Flame)

In previous studies, traditional analysis methods such as photomultiplier tubes were used, which treated the flame as a whole synchronous movement and then obtained the amplitude of the one−dimensional signal of flame pulsation. Nevertheless, the flame shows periodic pulsation under acoustic forcing. The present study introduced the DMD method to quantitatively calculate the flame pulsation amplitude. Figure 6 presents the comparison results, which indicate that the DMD method is more accurate than the one−dimensional processing. In addition, Figure 7 presents the results of some repeated measurements of Case A, which confirms the validity of the results in this study. With regard to FTF, more detailed frequency resolution is always desirable and the resulting curve is smoother [38,39]. However, this greatly increases the difficulty of the experiment. Based on the repeatability measurement results, the frequency step of this research is determined to be 20~30 Hz.

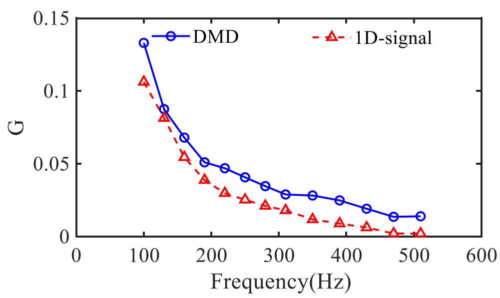

Figure 6. Comparison results in Case A (p_A = 0.1).

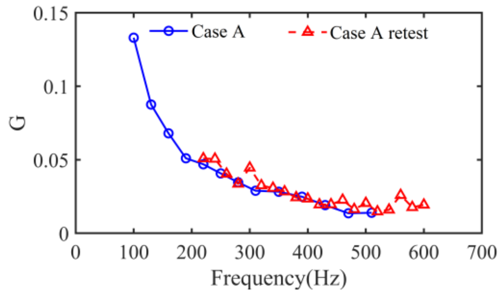

Figure 7. Repetitive test in Case A (p_A = 0.1).

The FDF analysis necessarily requires the use of small enough amplitudes of acoustic forcing disturbance to ensure that flame pulsation occurs in the linear region [40]. In the study of FTF, the dimensionless disturbance amplitude is 0.1. Combined with the FDF results listed below, the disturbance amplitude is small and close to the signal−to−noise ratio limit.

Figure 8 shows the amplitude gain and phase delay under different frequencies of forcing pressure pulsation. With increasing acoustic forcing frequency, the flame pulsation gain decreases rapidly and then stabilizes. This is distinct from most of the research results on velocity disturbance. When the velocity disturbance is taken as the input parameter, the flame pulsation gain curve often shows a fluctuating characteristic, which is generally related to the acoustic characteristics of the combustion system. In contrast, the gain curve of the pressure pulsation obtained in this section varies monotonically with frequency, and the pulsation amplitude tends to become stable when the frequency exceeds 500 Hz. The amplitude gain increases rapidly with decreasing frequency. The flow pulsations upstream of the swirler and the pulsation at the root of the flame have the lowest convection times (as shown in Figure 8B), and this greatly increases the possibilities for strong coupling between the heat release rate pulsation and the pressure pulsation. In view of this, the low−frequency pulsation of the combustor under analysis is detrimental to its combustion instability.

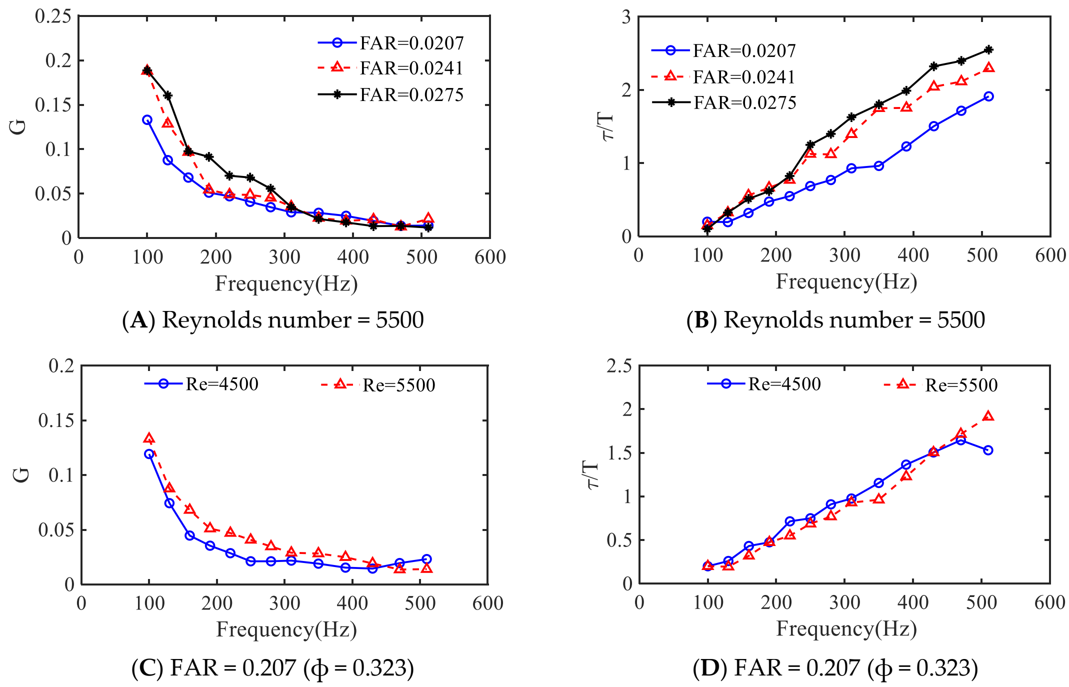

Figure 8. Flame pulsation transfer function (p_A = 0.1).

The FTF also presents an increasing trend, which benefits from the incremental flame front. However, this phenomenon is confined to the relatively low−frequency range. For example, in the case where the frequency exceeds 300 Hz, the effect of the equivalence ratio on the gain of FTF is weakened. The relative convection time presents significant differences with changes in equivalence ratio, and the flame pulsation has a reduced convection time under a lesser equivalence ratio, indicating a smaller phase difference. It is also known that the dynamic performance of flame pulsation differs under different Reynolds numbers, which means that the combustion instability problem is also seriously affected by the Reynolds number. Therefore, the present study evaluates the characteristics of flame under a constant acoustic forcing amplitude to reveal variation in combustion instability characteristics under different Reynolds numbers. The inlet Reynolds number has a relatively smaller effect on the convection time but affects the flame pulsation gain more. For larger Reynolds numbers, the heat release rate pulsation increases, and the acoustic forcing amplitude leads to a larger flame pulsation, given that the flame is also releasing its heat in a constant space. The amplitude of flame pulsation caused by high−frequency acoustic wave disturbance is relatively small; at these frequencies, the difference due to the Reynolds number is relatively insignificant.

In view of the sampling rate, the error of phase difference was relatively large at higher frequencies, so the resulting curve is not perfect. Although the results for Re = 4500 fall suddenly at 510 Hz, in fact, its rate of change with frequency is consistent with the Reynolds number of 5500. The sudden change at 510 Hz for Re = 4500 is attributed to experimental and calculation errors.

Firstly, the acoustic resonance of the combustion system was analyzed through finite element method numerical simulation to reveal the thermoacoustic coupling characteristics. The monopole acoustic source with an amplitude of 1 kg/s^2 was placed at the flame position to simulate the acoustic response. The number of mesh nodes is around 0.6 million; therefore, the maximum analyzable frequency is 3900. This research only analyzed the acoustic characteristics below 500 Hz, as the combustion instability occurring falls within the low−frequency region. The thermodynamic data of pressure and temperature were obtained through the CFD method. Figure 9 shows the temperature distribution and acoustic response of the self−excited combustion instability system. The presence of high temperature will increase the resonant frequency of the system. There are numerous resonant frequencies in the system, and the first resonance frequency is 166 Hz.

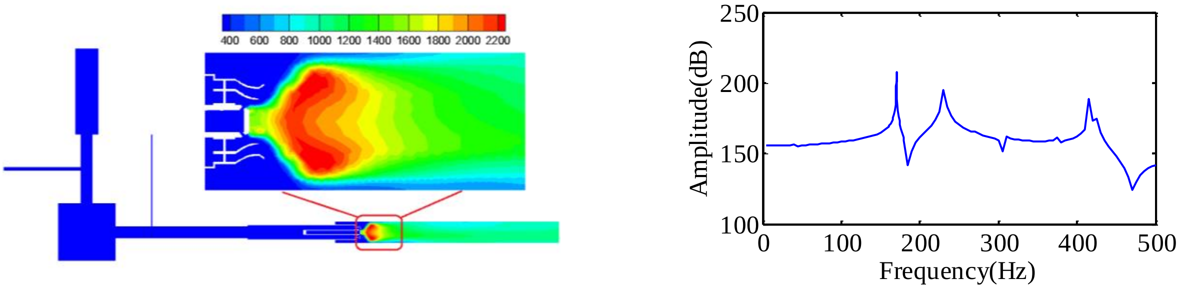

Figure 9. Temperature distribution (**left**) and acoustic response (**right**) of self−excited combustion instability system (L_c = 900 mm).

Then, self−excited combustion instability was generated when the combustion chamber length L_c was varied in Case A. Figure 10 shows the oscillation pressure amplitude and the dominant frequency under various geometrical conditions with constant air and fuel inlet conditions. The dominant frequency of oscillating pressure is 160 Hz at L_c = 900 mm. The results indicate that the oscillation frequency of the self−excited combustion instability in this study is close to the acoustic resonance frequency, which confirms the occurrence of thermoacoustic coupling in the system.

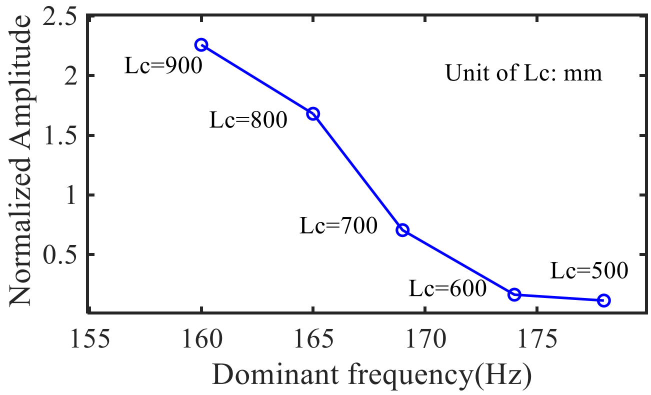

Figure 10. Pressure oscillation amplitude with different quartz glass combustion chamber lengths.

In addition, the dominant frequency increases with the decreasing of chamber length, while the amplitude reduces significantly. In this study, the FTF is used to explain the oscillation characteristics of self−excited combustion instability. It can be found from the FTF that the gain in flame pulsation decreases rapidly with the increasing of frequency; these tendencies reduce the feedback intensity of the flame pulsation at higher frequencies, which, in turn, weakens the strength of the self−exciting combustion instability.

3.2. FDF

Even though the present study analyzes the FDFs in a range that extends from 100 Hz to 510 Hz, these functions present a certain similarity across the frequency intervals. The main difference is whether there is a slowly growing triggering area in the initial stage. Figure 11 shows changes in the flame pulsation with amplitude change under two typical frequencies: 160 Hz represents the low−frequency band (less than 200 Hz), while 220 Hz represents the high−frequency band (greater than 200 Hz). The heat release rate pulsation amplitude is directly selected as the flame drive to reveal the complex and changing trend. The FTF from pressure follows a similar trend in this study and can better explain the internal mechanism of self−excited combustion instability.

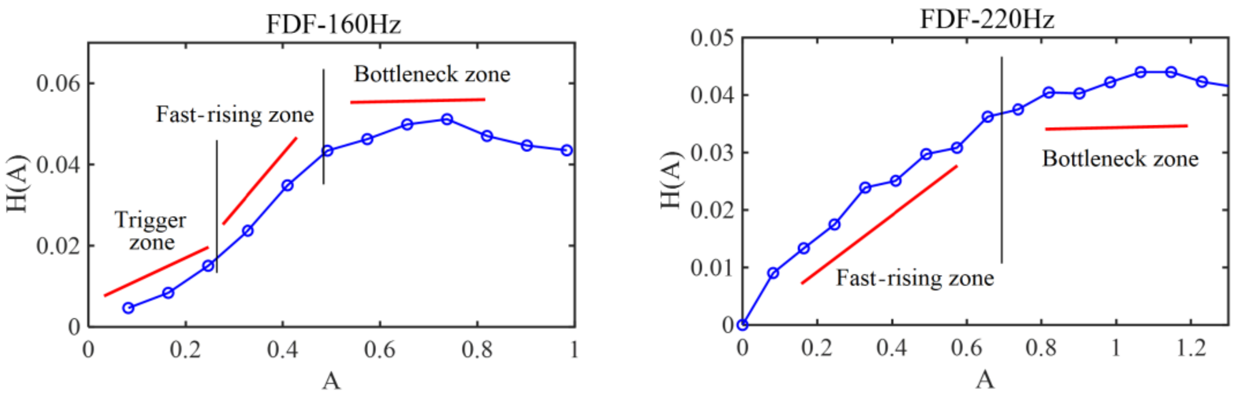

(**A**) Dominant frequency is 160 Hz (**B**) Dominant frequency is 220 Hz

Figure 11. Flame describing function (Case A, L_c = 100 mm).

Firstly, with the increase in the disturbance amplitude, the results indicate that the growth in heat output is mainly divided into three stages when the dominant frequency is lower than 200 Hz, i.e., the triggering stage, the fast−rising stage and the bottleneck stage. In the present study, there is no strict standard for the division of the growth process in the FDF at present. However, the FDF is recognizable at different frequencies from its curve. For instance, when there is a clear slow growth stage initially, the approximate position of the trigger zone can be determined. At the later stage of increasing pressure disturbance amplitude, once the flame driving growth has become weak, the growth is no longer obvious or even decreasing, and then the approximate position of the bottleneck stage can be determined.

The flame pulsation in the triggering area shows the negativity, the increasing amplitude of the flame pulsation is not evident and the heat release rate driving energy is generally small. In the fast−rising area, the flame pulsation undergoes growth. The driving energy of the heat release rate pulsation grows until reaching the peak, which is mainly attributed to the fact that the flame has reached its blow−out limit; at this point, the flame pulsation enters the bottleneck stage. Figure 11B shows that in the case of the frequency of acoustic forcing exceeding 200 Hz, the triggering area disappears and the induced heat release rate is mainly divided into the fast−rising stage and the bottleneck stage. With the increase in the amplitude of the pressure pulse, the growth velocity of the heat release rate amplitude decreases; however, the two cannot be distinguished due to the limitation of data acquisition resolution. Expressed as a time interval, the phase difference between the maximum amplitude and the minimum amplitude is within 0.5 ms and the relative convection time error is within 0.08.

3.3. Analysis of the Triggering of Combustion Instability

Figure 12A–C depict the changes in the heat release rate and damping dissipation at three typical frequencies (160 Hz, 220 Hz and 350 Hz, respectively). Energy dissipation mainly constitutes the damping of combustion instability. Acoustic waves transmit energy to the environment through the combustion system boundary. On the other hand, energy dissipation also occurs in the form of thermal energy loss. These two aspects are difficult to evaluate in quantitative terms and are usually simplified into linear curves by researchers [32]. In fact, the degree of damping dissipation can be deduced from the amplitude of the limit cycle state. In the present study, the linear damping curve was regarded as a hypothesis to be tested by analyzing the triggering mechanism of combustion instability in combination with the FDF. The results revealed the existence of a trigger threshold of pressure disturbance when the flame pulsation was in the triggering stage. The rate of growth of the heat release rate is relatively lower than the rate of growth velocity of the pressure disturbance amplitude, and it is thus difficult to balance the damping dissipation. Only when the oscillation pressure amplitude exceeds the trigger threshold can it promote the self−sustaining increase in heat release rate amplitude and pressure oscillation, so combustion instability can then take hold and build up to the limit cycle state. Figure 12B shows a frequency at which the trigger threshold does not exist, so the growth of heat pulsations only presents the fast−growing stage and the bottleneck stage. Figure 12C shows that if the driving slope at amplitude zero is less than the damping dissipation, the rate of heat output buildup in each pulsation is still less than the dissipation as the oscillation pressure amplitude increases, and the system is stable. For the model combustor fed with a butane diffusion flame studied in this paper, the stabilizing effect was particularly prominent and typical at frequencies above 350 Hz.

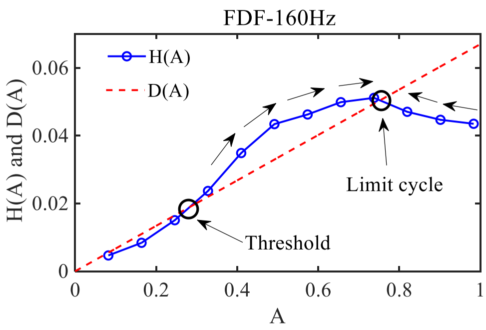

(**A**) FDF−160Hz

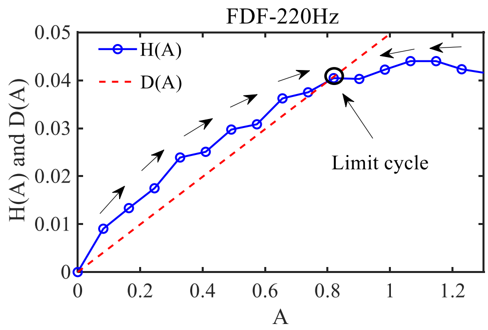

(**B**) FDF−220Hz

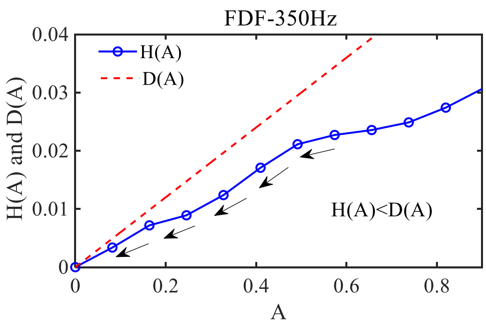

(**C**) FDF−350Hz

Figure 12. Flame drive growth model under three forcing frequencies.

3.4. Analysis of the Self−Excited Limit Cycle

During the present study, marked combustion instabilities were created by changing the inlet conditions and the combustion chamber length. Although the oscillation intensity varied greatly, the experiment maintained a dominant frequency of oscillation of a fundamentally constant nature, which was extremely useful for understanding and verifying the processes through which combustion instability is triggered. The dominant acoustic frequency was closely related to the combustion system. The dominant acoustic frequency fell between 160 and 174 Hz over the range of combustion chamber lengths that ran from 500 to 900 mm. It may be said of our experimental system that the dominant frequency of combustion instability did not change markedly and is approximately 160 Hz.

From the drive dissipation model shown in Figure 12A, under strong coupling oscillation, the oscillation pressure and heat release rate pulsation are stable at the limit cycle state, and the flame pulsation is often in the bottleneck period. Figure 13 presents the pressure pulsation amplitude and the relative convection time during combustion instability under different working conditions. The oscillatory condition of the combustion instability is now generally divided into two categories, i.e., the limited state and the limit cycle state. Combustion instability under the limited state and under the limit cycle state is expressed by the blue circle and the red triangle, respectively. The boundary of oscillation states is evident. The pressure oscillation amplitude under the limited state is lower than 0.2, while the convection time is generally greater than 0.4. The pressure oscillation amplitude under the limit cycle state is generally greater than 0.4, but the convection time is relatively short and tends to decrease with the increasing oscillation amplitude. The point marked with a black box is the shortest working point of the combustion chamber, with a smaller pressure oscillation amplitude and a shorter convection time, which was attributed to the fact that the geometric construction ensures a smaller sound pressure feedback at this position in the flame.

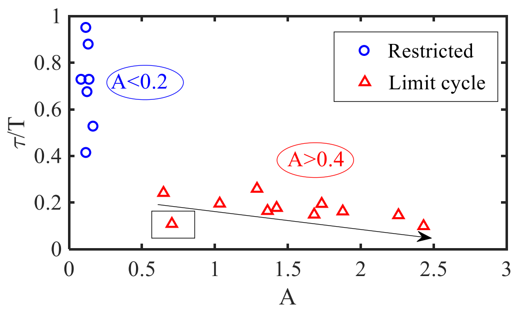

Figure 13. Drive dissipation model and oscillation state.

The results described so far reveal a critical amplitude between the trigger stage and the rapid rise stage, i.e., the trigger threshold, which is an inflection point. Below this threshold, flame pulsation grows only slowly with increasing oscillation pressure amplitude, and the driving energy of the heat release rate is lower than the dissipated energy. The driving energy of the heat release rate balances the dissipated energy at the trigger threshold. The pressure pulsation amplitude corresponding to 0.2 falls in the trigger phase of the drive dissipation model, while the amplitude at 0.4 is within the rapid rise period, indicating that two kinds of combustion instability in Figure 13B belong to the trigger phase and the bottleneck phase. The results of this study seem to show that pressure pulsation is a common phenomenon, although strongly coupled oscillation does not occur. For instance, when the flame pulsation shows negativity with increasing levels of oscillation pressure amplitude, the heat release rate pulsation does not cause further increases in pressure pulsation, and under these conditions, the combustion instability is always within the trigger phase. Figure 14 shows the corresponding pressure wave in the time domain. Over this period, the oscillation pressure amplitude maintains a lower level, and the pressure signal generated by combustion instability is in a limited state. The pressure wave is subject to strong instability, and the amplitude is always maintained within 0.4. When the flame shows positivity, the amplitude increase exceeds the trigger threshold, after which the flame pulsation enters the bottleneck stage, and the combustion instability becomes stable in the limit cycle state.

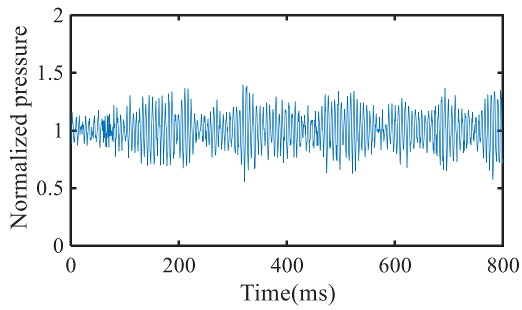

Figure 14. Pressure under combustion instability in the limited state (f = 166 Hz, L_c = 900 mm).

The convection time in Figure 13B further indicates that the relative convection time is below 0.3 when the combustion instability is stabilized in the limit cycle state, while it is generally greater than 0.4 in the limited state. Combined with the FTF, the frequency with a lower convection time is below 300 Hz. Hence, even if there is a high resonance frequency, combustion instability with a dominant frequency above 300 Hz does not occur.

3.5. Pressure Growth Process

The supplies of air and fuel were first adjusted to trigger the combustion instability, with the equivalence ratio sufficiently lean to ensure the self−exciting combustion instability. The combustor was then ignited, allowing increases in the oscillation pressure amplitude and flame pulsation to build up under experimental observation. Figure 15 shows the unsteady progress of the pressure pulsations and heat release rate pulsations, including the fast−growing phase and the transition to steady−state phase. The initial flame produces pressure expansion. Then, the pressure wave is reflected to the flame position through the combustor boundary, further interfering with the flame and generating the pulsation. The coupling and gain further increase the amplitude of the pressure pulsation and the heat release rate pulsation. In the later period, the flame pulsation fails to satisfy the dissipation energy required for further increase in amplitude as it approaches the limit of flame pulsation, and so the amplitude reaches its peak. Then, the system enters a transition to the steady−state phase. However, it is worth noting that the limit cycle state does not mean that the amplitude remains stable but that the system is interfered with by the flow and the phase mutation exists in the flame pulsation, which leads to the fluctuation of the combustion instability system within the steady−state period, so the amplitude of pressure pulsation and heat release rate pulsation still fluctuate to a certain extent.

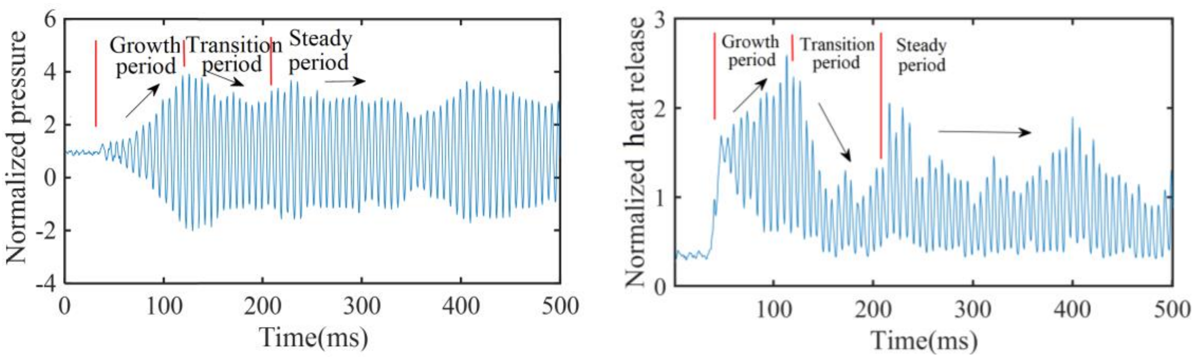

(**A**) Pressure (**B**) Heat release rate

Figure 15. Growth process of pressure signal and heat release rate pulsation signal.

The growth rate in this research represents the initial growth of oscillating pressure, and it is experimentally derived from the slope fitting of acoustic pressure. This is similar to the growth rate defined in the literature [32] and can be converted to each other. The definition of Equation (6) in this manuscript is determined to obtain a better fitting of the pressure pulsation envelope. The growth rate is a real value, where a positive value denotes the growth of the acoustic disturbance, and the combustion system is stable when the growth rate is equal to 0. To obtain the envelope of the pressure signal, it was first required to find the maximum point and the minimum point of the dynamic pressure signal. Then, a spline interpolation was performed three times for the maximum point or minimum point, as shown in Figure 16, to obtain the envelope of the dynamic pressure signal, which reflects the change in amplitude of the dynamic pressure. Figure 17 presents the results of this exponential fit. The fitting data length is 100 ms, and its initial position is firstly determined by the initial growth rate, which is set as 10 Pa/s, to ensure the consistency of the initial growth rate of the pressure signal under different working conditions. At the initial point of the fitting data, the amplitude of oscillation pressure presents an increasing trend and has a relatively small growth rate. The growth rate $A'(t_0)$ is then obtained in the position 25 ms after the initial fitting point to evaluate the growth rate of the oscillation pressure amplitude in the growth phase under different working conditions.

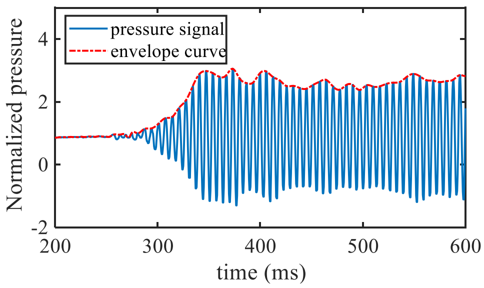

Figure 16. Establishment of the pressure signal envelope.

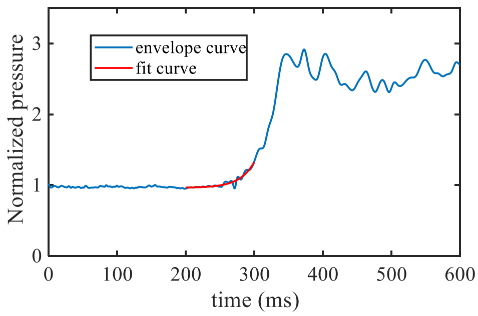

Figure 17. Exponential fitting of the pressure signal envelope.

Figure 18 presents the growth rate of the oscillation pressure amplitude within the growth phase. As mentioned above, the dominant frequency increases after shortening the combustion chamber length, and the flame pulsation has a relatively smaller amplitude gain. In addition, the flame pulsation possesses a relatively smaller acoustic pressure response amplitude. Similarly, the heat release rate pulsation caused by the acoustic forcing will lead to smaller pressure feedback, thereby causing a decrease in the growth rate of oscillation pressure amplitude with increasing combustion chamber length. Additionally, a larger Reynolds number produces a greater amplitude growth rate. The airflow velocity is far lower than the velocity of sound, and the increase in Reynolds number will not cause a significant change in the acoustic characteristics of the combustor. Hence, the increase in pressure and heat release rate feedback intensity caused by a larger Reynolds number are mainly a product of the growth of flame gain with an increasing Reynolds number. It is noteworthy that the growth rate decreases when L_c = 900 mm. However, the oscillation pressure amplitude reaches its maximum value under the limit cycle state, a fact that reflects the particularity of the pressure pulsation and heat release rate pulsation feedback process during the growth period. The concept of the attractor structure in chaos theory is then adduced to further explain the phase space trajectory of the feedback process in the growth period.

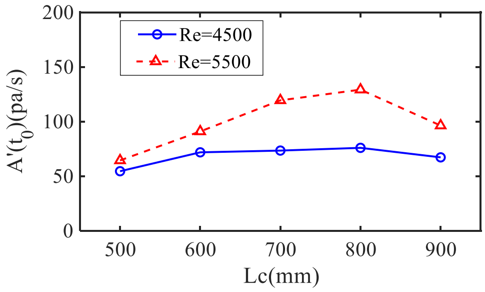

Figure 18. Growth rate of oscillation pressure amplitude in the growth period.

3.6. Coupling Growth between the Heat Release Rate Pulsation and the Pressure Pulsation

In terms of the physical quantities in the kinematic equation, the multidimensional trajectory formed by each physical quantity in the kinematic equation denotes a phase space trajectory; the attractor structure reveals the coupling and joint growth between the pressure pulsation and the heat release rate pulsation. Figure 19 describes the attractor structure of the pressure pulsation and the heat release rate fluctuation within the growth period. In the initial state, the pressure pulsations and the heat release rate pulsations are in the background noise, and the phase space trajectory presents the disordered motion. After successful ignition, the system will enter the growth period and develop toward a regime of orderly movement. Burned gas absorbs heat and expands, further increasing the pressure disturbance. The pressure disturbance thus generated then affects the combustion heat release rate in the flame after being reflected by the combustion chamber boundary. Then, the heat release rate pulsation exhibits a degree of gain from the pressure fluctuation.

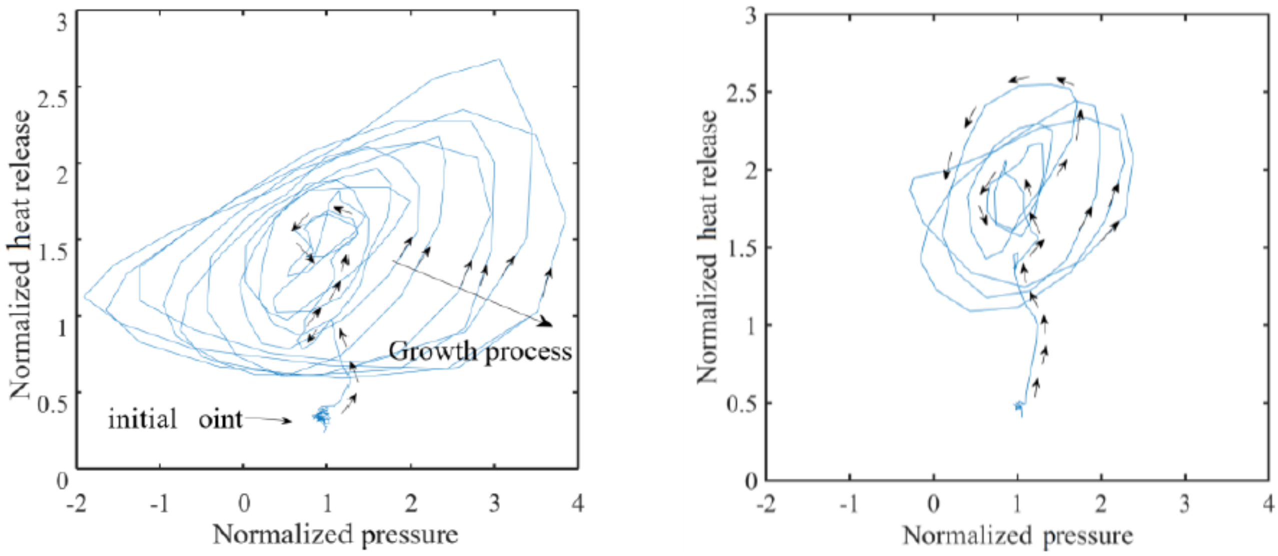

(**A**) L_c = 900 mm (**B**) L_c = 800 mm

Figure 19. Attractor structures within the growth period.

The attractor structure reflects the phase changes of the pressure pulsation and heat release rate pulsation within the growth period. For the case of L_c = 900 mm, it takes four cycles to enter the stable orbit, while for the case of L_c = 800 mm, it takes about three cycles. The phase difference change in the above analysis explains the growth process of the pressure amplitude in the growth period. In the initial period, the phase difference is relatively large, while the growth rate of the amplitude is relatively low. The amplitude growth rate increases with decreasing phase difference. Finally, the amplitude growth slows down until the saturation state (the limit cycle state) is attained, the state which is limited by the FDF. From the period of entering the stable orbit, when the combustion chamber length is 900 mm, the system has a relatively long period, which indicates that although the amplitude of pressure oscillation is small, it has a fast amplitude growth rate benefiting from the short combustion chamber length. The early coupling or the establishment of the resonance state is influenced by the propagation time of the sound wave in the combustion chamber.

Figure 20 shows the attractor structure during the entire triggering phase; it presents a degree of confusion, which is mainly caused by the random characteristics of the self−exciting combustion instability process. Various forms of interference make the heat release rate pulsation prone to generating phase mutation and random characteristics. The black dot is the approximate center of the trajectory. The central point of the attractor structure is deflected in the steady−state period due to the transition period, and the attractor structure is found to show the motion orbit. However, its structure is not a perfect oval because the heat release rate pulsations are subject to non−linear fluctuations, with the result that it has a waveform that deviates from the sinusoidal through a superimposed ripple. In addition, a deflection angle between the steady−state attractor structure and the growth attractor structure is also evident. No phase relation has been established between the pressure pulsation and heat release rate pulsation within the growth period. However, this phase relation may adjust in the transition period and tends to be stable in the steady−state period.

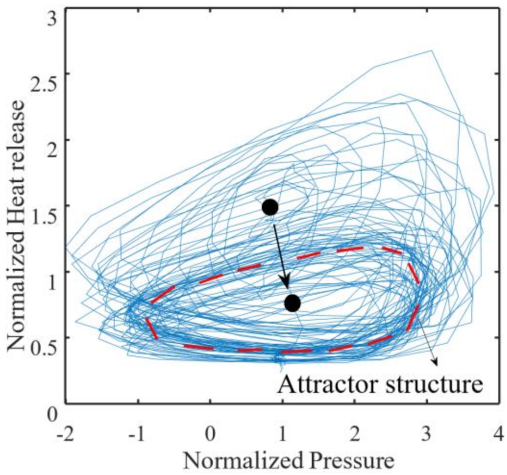

Figure 20. Attractor structure of the triggering phase (L_c = 900 mm).

4. Conclusions

The triggering mechanism of combustion instability is hereby studied, instability that mainly consists of two states, i.e., the limited state and the limit cycle state. The triggering mechanism explains the reasons for the combustion instability. The main conclusions are as follows:

(1) The flame pulsation gain G at different frequencies is below 0.2 under the conditions investigated, which shows the monotonic decreasing trend with frequency and an increasing trend with Reynolds number and FAR. However, the relative convection time decreases with the increase in the inlet Reynolds number and increases with the increase in FAR. Therefore, the increase in the inlet Reynolds number is unfavorable to combustion instability. In addition, the self−excited combustion oscillation intensity of the combustion system is sustained by the feedback amplitude of the acoustic disturbance at the location of the flame.

(2) The flame pulsation amplitude shows a complex curvature when the frequency is lower than 200 Hz, while the growth rate monotonically decreases for frequencies greater than 200 Hz. According to the considerable self−excited combustion instability tests under different working conditions, the oscillation amplitudes in the limit cycle state are generally greater than 0.4, while the pressure amplitudes in the limited state are less than 0.2, thus verifying the concept of a trigger threshold for low−frequency oscillation.

(3) The growth process of combustion instability is divided into a growth period, a transition period and a steady−state period. Attractor theory confirmed the process of gradual coupling between the acoustic pressure and the heat release rate pulsation. During this stage, the flame caused by the initial ignition produces a pressure expansion that is reflected to the flame from the wall of the combustion chamber to further interfere with the flame and generate the pulsation. The mutual coupling and gains further increase the amplitude of the pressure pulsation and heat release rate pulsation.

Author Contributions: Conceptualization, Y.L. and Y.Y.; methodology, S.S.; validation, H.M. All authors have read and agreed to the published version of the manuscript.

Funding: This work received funding from the National Major Science and Technology Projects of China (J2019-III-0004-0047).

Data Availability Statement: All data supporting reported results can be found, including links to publicly archived datasets analyzed or generated during this study.

Conflicts of Interest: All authors disclosed no relevant relationship.

References

1. Lieuwen, T.C.; Yang, V.; Lu, F. Combustion instabilities in gas turbine engines: Operational experience, fundamental mechanisms and modeling. *Am. Inst. Aeronaut. Astronaut.* **2006**, *866807*, 29–41.
2. Guan, Y.; Becker, S.; Zhao, D.; Xu, J.; Shahsavari, M.; Schluter, J. Entropy generation and CO_2 emission in presence of pulsating oscillations in a bifurcating thermoacoustic combustor with a Helmholtz resonator at off−design conditions. *Aerosp. Sci. Technol.* **2023**, *136*, 108204. [CrossRef]
3. Zhao, D. *Thermoacoustic Combustion Instability Control, Engineering Applications and Computer Codes*; Academic Press: Cambridge, MA, USA, 2023; pp. 513–583.
4. Liu, Y.; Li, J.; Zhang, T.; Yan, Y. Active suppression of swirl−stabilized combustion instability. *Fuel* **2021**, *287*, 119559. [CrossRef]
5. Liu, Z.; Zhou, H.; Wei, D.; Fang, H. Experimental research on using CO2−Ar microjets to control liquid fuel combustion instability and pollutant emission. *J. Energy Inst.* **2021**, *98*, 346–353. [CrossRef]
6. Liu, Z.; Zhou, H.; Fang, H.; Tao, C. Suppression of combustion instabilities of swirled non−premixed liquid−fuel flame with CO_2-O_2 jet in cross−flow. *J. Energy Inst.* **2021**, *95*, 69–76. [CrossRef]
7. Zhao, D. A real−time plane−wave decomposition algorithm for characterizing perforated liners damping at multiple mode frequencies. *J. Acoust. Soc. Am.* **2011**, *129*, 1184–1192. [CrossRef]
8. Zhao, D.; Gutmark, E.; Reinecke, A. Mitigating self−exited flame pulsating and thermoacoustic oscillations using perforated liners. *Sci. Bull.* **2019**, *64*, 941–952. [CrossRef]
9. Thumuluru, S.K.; Lieuwen, T. Characterization of acoustically forced swirl flame dynamics. *Proc. Combust. Inst.* **2009**, *32*, 2893–2900. [CrossRef]
10. Yoon, M. Combustion instability analysis from the perspective of acoustic impedance. *J. Sound Vib.* **2020**, *483*, 115500. [CrossRef]
11. Ducruix, S.; Schuller, T.; Durox, D.; Candel, S. Combustion dynamics and instabilities: Elementary coupling and driving mechanisms. *J. Propuls. Power* **2003**, *19*, 722–734. [CrossRef]
12. Sun, Y.; Zhao, D.; Ji, C.; Zhu, T.; Rao, Z.; Wang, B. Large−eddy simulations of self−excited thermoacoustic instability in a premixed swirling combustor with an outlet nozzle. *Phys. Fluids* **2022**, *34*, 044112. [CrossRef]
13. Di, D.; Yan, Y.; Liu, Y. Study on the flow characteristics and oscillating mechanism of a swirl flame. *Fuel* **2021**, *306*, 121657. [CrossRef]
14. Cheng, Y.; Jin, T.; Luo, K.; Li, Z.; Fan, J. Large eddy simulations of spray combustion instability in an aero−engine combustor at elevated temperature and pressure. *Aerosp. Sci. Technol.* **2021**, *108*, 106329. [CrossRef]
15. Song, X.; Zhu, T.; Pan, D.; Wang, Z.; Ji, C.; Zhao, D. Numerical investigations on the beating behavior of self−excited combustion instability in a hydrogen−fueled Rijke type combustor. *Aerosp. Sci. Technol.* **2022**, *126*, 107624. [CrossRef]
16. Murthy, S.R.; Sayadi, T.; Le Chenadec, V.; Schmid, P.J.; Bodony, D.J. Analysis of degenerate mechanisms triggering finite−amplitude thermo−acoustic oscillations in annular combustors. *J. Fluid Mech.* **2019**, *881*, 384–419. [CrossRef]
17. Liu, Z.; Wei, D.; Ji, M.; Fang, H.; Zhou, H. Combustion instability of ethanol and n−heptane fuels under different combustor geometries. *J. Energy Inst.* **2022**, *102*, 206–215. [CrossRef]
18. Liu, Y.; Li, J.; Han, Q.; Yan, Y. Study of combustion oscillation mechanism and flame image processing. *AIAA J.* **2019**, *57*, 824–835. [CrossRef]
19. Zhao, H.; Li, G.; Zhao, D.; Zhang, Z.; Sun, D.; Yang, W.; Li, S.; Lu, Z.; Zheng, Y. Experimental study of equivalence ratio and fuel flow rate effects on nonlinear thermoacoustic instability in a swirl combustor. *Appl. Energy* **2017**, *208*, 123–131. [CrossRef]
20. Zhang, Z.; Zhao, D.; Ni, S.; Sun, Y.; Wang, B.; Chen, Y.; Li, G.; Li, S. Experimental characterizing combustion emissions and thermodynamic properties of a thermoacoustic swirl combustor. *Appl. Energy* **2019**, *235*, 463–472. [CrossRef]
21. Joo, S.; Choi, J.; Lee, M.; Kim, N. Prognosis of combustion instability in a gas turbine combustor using spectral centroid & spread. *Energy* **2021**, *224*, 120180.
22. Kim, T.; Ahn, M.; Lim, D.; Yoon, Y. Flame describing function and combustion instability analysis of non−premixed coaxial jet flames. *Exp. Therm. Fluid Sci.* **2022**, *136*, 110642. [CrossRef]
23. Alabaş, B. Effect of biogas addition on combustion instability of propane flame at different external acoustic enforcement frequencies. *Fuel* **2022**, *317*, 123498. [CrossRef]
24. Hermeth, S.; Staffelbach, G.; Gicquel LY, M.; Anisimov, V.; Cirigliano, C.; Poinsot, T. Bistable swirled flames and influence on flame transfer functions. *Combust. Flame* **2014**, *161*, 184–196. [CrossRef]

25. Zhu, R.; Pan, D.; Ji, C.; Zhu, T.; Lu, P.; Gao, H. Combustion instability analysis on a partially premixed swirl combustor by thermoacoustic experiments and modeling. *Energy* **2020**, *211*, 118884. [CrossRef]
26. Xia, Y.; Laera, D.; Jones, W.P.; Morgans, A.S. Numerical prediction of the Flame Describing Function and thermoacoustic limit cycle for a pressurised gas turbine combustor. *Combust. Sci. Technol.* **2019**, *191*, 979–1002. [CrossRef]
27. Wang, Y.; Sohn, C.H.; Bae, J.; Yoon, Y. Prediction of combustion instability by combining transfer functions in a model rocket combustor. *Aerosp. Sci. Technol.* **2021**, *119*, 107202. [CrossRef]
28. Xu, L.; Zheng, J.; Wang, G.; Li, L.; Qi, F. Effects of swirler position on flame response and combustion instabilities. *Chin. J. Aeronaut.* **2022**, *35*, 345–355. [CrossRef]
29. Campa, G.; Camporeale, S.M.; Cosatto, E.; Mori, G. Thermoacoustic analysis of combustion instability through a distributed flame response function. In Proceedings of the ASME Turbo Expo 2012, Copenhagen, Denmark, 11–15 June 2012; American Society of Mechanical Engineers: New York, NY, USA, 2012. paper GT2012−68243; 2, PTS A AND B: 2012.
30. Han, X.; Li, J.; Aimee, S. Prediction of combustion instability limit cycle oscillations by combing flame describing function simulations with a thermoacoustic network model. *Combust. Flame* **2015**, *162*, 3632–3647. [CrossRef]
31. Eirik, A.; Indlekofer, T.; Gant, F.; Cuquel, A.; Bothien, M.R.; Dawson, J.R. The effect of hydrogen enrichment, flame−flame interaction, confinement, and asymmetry on the acoustic response of a model can combustor. *Combust. Flame* **2022**, *242*, 112176.
32. Kim, K.T.; Hochgreb, S. Measurements of triggering and transient growth in a model lean−premixed gas turbine combustor. *Combust. Flame* **2012**, *159*, 1215–1227. [CrossRef]
33. Wang, G.; Zheng, J.; Li, L.; Liu, X.; Qi, F. Relationship of gain and phase in the transfer function of swirling flames. *Proc. Combust. Inst.* **2021**, *38*, 6173–6182. [CrossRef]
34. Oberleithner, K.; Schimek, S.; Paschereit, C.O. Shear flow instabilities in swirl−stabilized combustors and their impact on the amplitude dependent flame response: A linear stability analysis. *Combust. Flame* **2015**, *162*, 86–99. [CrossRef]
35. Æsøy, E.; Nygård, H.T.; Worth, N.A.; Dawson, J.R. Tailoring the gain and phase of the flame transfer function through targeted convective−acoustic interference. *Combust. Flame* **2022**, *236*, 111813. [CrossRef]
36. Schmid, P.J. Dynamic mode decomposition of numerical and experimental data. *J. Fluid Mech.* **2010**, *656*, 5–28. [CrossRef]
37. Zhao, D. System identification and impulse response of a methane−fuelled swirling thermoacoustic combustor. *Therm. Sci. Eng. Prog.* **2023**, *37*, 101575. [CrossRef]
38. Rao, Z.; Li, R.; Zhang, B. Nonlinear dynamics of a swirl−stabilized combustor under acoustic excitations: Influence of the excited combustor natural mode oscillations. *Flow Turbul. Combust.* **2012**, *107*, 683–708. [CrossRef]
39. Messineo, J.; Lestrade, J.Y.; Hijlkema, J.; Anthoine, J. Vortex shedding influence on hybrid rocket pressure oscillations and combustion efficiency. *J. Propuls. Power* **2016**, *32*, 1386–1394. [CrossRef]
40. Zhao, D. Thermodynamics−acoustics coupling studies on self−excited combustion oscillations maximum growth rate. *J. Therm. Sci.* **2022**, *31*, 1591–1603. [CrossRef]